Nematic-Orbit Coupling and Nematic Density Waves in Spin-1 Condensates

Di Lao,* Chandra Raman, and C. A. R. Sá de Melo
School of Physics, Georgia Institute of Technology, Atlanta, Georgia 30332, USA

(Received 1 April 2019; revised manuscript received 18 March 2020; accepted 13 April 2020; published 29 April 2020)

We propose the creation of artificial nematic-orbit coupling in spin-1 Bose-Einstein condensates, in analogy with spin-orbit coupling. Using a suitably designed microwave chip, the quadratic Zeeman shift, normally uniform in space, can be made to be spatiotemporally varying, leading to a coupling between spatial and nematic degrees of freedom. A phase diagram is explored where three quantum phases with the nematic order emerge: easy axis, easy plane with single-well structure, and easy plane with double-well structure in momentum space. By including spin-dependent and spin-independent interactions, we also obtain the low energy excitation spectra in these three phases. Last, we show that the nematic-orbit coupling leads to a periodic nematic density modulation in relation to the period λ_T of the cosinusoidal quadratic Zeeman term. Our results point to the rich possibilities for manipulation of tensorial degrees of freedom in ultracold gases without requiring Raman lasers, and therefore, obviating light-scattering induced heating.

DOI: 10.1103/PhysRevLett.124.173203

Ultracold atoms are a unique platform for exploring multifaceted quantum magnetic behavior associated with spin. Some of the success stories in this arena include spinor Bose-Einstein condensates (BECs) [1], where magnetic interactions play an important role, as well as systems with artificial spin-orbit coupling [2–13], where independent-particle effects are primarily involved. Yet a comprehensive experimental framework linking these two disparate regimes of spin physics in ultracold gases has been lacking. In part, this is due to the fact that some of the richest behavior in spinor gases involves the dynamics of spin-nematic phases [14–26]. These phases are special because they have a vanishing total magnetization vector $\langle\hat{\mathbf{F}}\rangle = 0$ and their order parameter is tensorial. For a spin-1 system, the expectation value of the spin-quadrupole tensor operator $\hat{\mathbf{Q}}_{ij} = \frac{1}{2}(\hat{\mathbf{F}}_i\hat{\mathbf{F}}_j + \hat{\mathbf{F}}_j\hat{\mathbf{F}}_i)$ may act as an order parameter, where i, j are the $\{x, y, z\}$ components of the spin operator $\hat{\mathbf{F}}$ [27]. Through interactions between atoms, such tensor objects naturally generate spin entanglement and strong correlations. An important example of this is the reaction between two $|F = 1, m = 0\rangle$ alkali atoms through s-wave scattering, that is $|1, 0\rangle + |1, 0\rangle \leftrightarrow |1, 1\rangle + |1, -1\rangle$, which conserves $m_1 + m_2 = 0$ of atoms 1 and 2 [28–33]. By contrast, the spin-orbit coupling achieved using Raman laser schemes does not readily lend itself to the study of pure spin-nematic objects, although a variety of other interacting many-body phases have been predicted [34–39].

In contrast to spin-orbit coupling, in this work we explore nematic-orbit coupling, where the linear momentum of spin-1 bosonic atoms is coupled to the spin-nematic degrees of freedom. Nematic spinor states have a zero expectation value for the spin vector $\langle\hat{\mathbf{F}}\rangle$ and nonzero quadrupole tensor $\langle\hat{\mathbf{Q}}_{ij}\rangle = \delta_{ij} - d_i d_j$, where $\mathbf{d}$ is the director. Easy-axis or easy-plane states correspond to $\mathbf{d}$ aligned with either the z direction or lying in the xy plane, respectively. Here, we propose an experimental setup to create nematic-orbit coupling between the center of mass of spin-1 bosons and the zz component of the spin-quadrupolar operator $\hat{\mathbf{Q}}_{zz} = \hat{\mathbf{F}}_z^2$, as shown in Fig. 1.

In the setup shown in Fig. 1, a spatiotemporally varying quadratic Zeeman shift $q(\mathbf{r}, t)\hat{\mathbf{F}}_z^2$ is created using a combination of a static bias field and a microwave field that is produced by a monolithic microwave integrated circuit [41]. After eliminating constant and linear terms in $\hat{\mathbf{F}}_z$ (see [40]), the effective independent-particle Hamiltonian is

$$\hat{H}_{\rm IP} = \int d\mathbf{r} \sum_a \psi_a^\dagger(\mathbf{r}) \left[\frac{\mathbf{p}^2}{2m}\hat{\mathbf{1}} + V(\mathbf{r})\hat{\mathbf{1}} + q(\mathbf{r}, t)\hat{\mathbf{F}}_z^2\right]\psi_a(\mathbf{r}), \tag{1}$$

where $\psi_a^\dagger(\mathbf{r})$ is the creation operator of bosons at position $\mathbf{r}$ with spin components $a = \{\pm 1, 0\}$, $\mathbf{p}^2/2m$ is the kinetic energy, $V(\mathbf{r}) = V_{\rm trap}(z)$ is the trap potential, $q(\mathbf{r}, t) = q + 2\Omega_c(z)\cos(k_T x - \omega t)$ is the resulting spatiotemporal modulation of the quadratic Zeeman shift with period $\lambda_T = 2\pi/k_T$, and $\hat{\mathbf{1}}$ is the identity matrix. The modulation amplitude $\Omega_c(z) = \Omega_0 + \Omega_1 z$ defines the strength of the nematic-orbit coupling. Since $\Omega_c(z)$ varies linearly with the z coordinate, it couples two discrete energy levels ϵ_1, ϵ_2 with different parity, which are defined by the spin-independent trapping potential $V(\mathbf{r})$. A resonance condition for the magnetic traveling wave can be achieved when

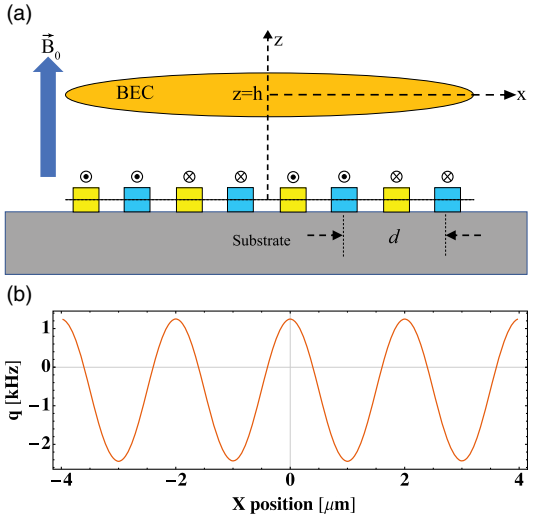

FIG. 1. Protocol for nematic-orbit coupling. (a) Optically trapped Bose-Einstein condensate at a height h above the centroid of a coplanar waveguide array. The array is part of a monolithic microwave integrated circuit that modulates the quadratic Zeeman shift $q(\mathbf{r},t)$ through the ac Zeeman effect. Two interleaved sets of wires (yellow and blue) are energized with microwave currents whose amplitude is modulated in proportion to $\cos\omega t$ and $\sin\omega t$, respectively. The result is a magnetic traveling wave creating a quadratic shift that varies nearly cosinusoidally as $q+\Omega_c(z)\cos(k_T x-\omega t)$. ω is near resonance with the confinement along z, as discussed in [40]. The spacing of each wire array is $d=2$ μm, a static field is $B_0=1.4$ G and a microwave field amplitude of $B_1=0.1$ G results from a current density amplitude per wire of 8.4×10^4 A/cm^2. The microwave frequency is detuned by $\Delta=+2$ MHz from the clock transition $|F=1,m_F=0\rangle\rightarrow|F=2,m_F=0\rangle$ at 1.77 GHz for ^{23}Na. (b) Plot of $q(x,z=h,t=0)$ at $h=2.5$ μm with $q=-600$ Hz, $\Omega_c(h)=1840$ Hz, and $k_T=2\pi/(2\ \mu\text{m})$.

$\omega\approx\omega_{12}\equiv(\epsilon_2-\epsilon_1)/\hbar$ [40]. Given the discrete nature of the spectrum along z, we write the field operators as $\psi_a(\mathbf{r})=\sum_n\varphi_n(z)\psi_{n,a}(x,y)$, where $\varphi_n(z)$ is the eigenfunction of trap state $n=\{1,2\}$. Within the rotating wave approximation and zero detuning $\omega-\omega_{12}=0$, the Hamiltonian can then be rewritten in momentum space as (see [40]):

$$\hat{H}_{\rm IP}=\sum_{\mathbf{k}_\perp n}\hat{\phi}^\dagger_{\mathbf{k}_\perp n}\mathbf{H}_D\hat{\phi}_{\mathbf{k}_\perp n}+[\Omega\hat{\phi}^\dagger_{\mathbf{k}_-,1}\hat{\mathbf{F}}_z^2\hat{\phi}_{\mathbf{k}_+,2}+\text{H.c.}]. \tag{2}$$

Here, $\hat{\phi}^\dagger_{\mathbf{k}_\perp n}=[\phi_{n,1}(\mathbf{k}_\perp),\phi_{n,0}(\mathbf{k}_\perp),\phi_{n,\bar{1}}(\mathbf{k}_\perp)]$ is the spinor creation operator with subscript $\bar{1}$ as a shorthand for -1, $\mathbf{k}_\perp=(k_x,k_y)$, $\mathbf{H}_D=\varepsilon_{\mathbf{k}}\hat{\mathbf{1}}+q\hat{\mathbf{F}}_z^2$, where $\varepsilon_{\mathbf{k}}=\hbar^2k_\perp^2/(2m)$ is the kinetic energy with $k_\perp=|\mathbf{k}_\perp|$, and $\mathbf{k}_\pm=\mathbf{k}_\perp\pm(k_T/2)\hat{\mathbf{x}}$ are shifted momenta. The Hermitian conjugate (H.c.) term is $\Omega\hat{\phi}^\dagger_{\mathbf{k}_+,2}\hat{\mathbf{F}}_z^2\hat{\phi}_{\mathbf{k}_-,1}$, where $\Omega=\int dz\varphi_1^*(z)[\Omega_1 z]\varphi_2(z)$ plays the role of a Rabi frequency (see [40]). The diagonalization of Eq. (2) leads to a trivial eigenvalue $E_0=\hbar^2k_\perp^2/(2m)$ corresponding to spin component $a=0$, and to nontrivial eigenvalues

$$E_{\alpha,\beta}(\mathbf{k}_\perp)=q+\frac{\hbar^2}{2m}\left[k_\perp^2+\frac{1}{4}k_T^2\right]\pm\sqrt{\left[\frac{\hbar^2}{2m}k_xk_T\right]^2+\Omega^2}. \tag{3}$$

The lower (higher) energy branch is labeled by $\alpha(\beta)$, with corresponding eigenvectors

$$\begin{pmatrix}\chi_{a\alpha}(\mathbf{k}_\perp)\\ \chi_{a\beta}(\mathbf{k}_\perp)\end{pmatrix}=\begin{pmatrix}u_{+\alpha}(\mathbf{k}_\perp) & u_{-\alpha}(\mathbf{k}_\perp)\\ u_{+\beta}(\mathbf{k}_\perp) & u_{-\beta}(\mathbf{k}_\perp)\end{pmatrix}\begin{pmatrix}\phi_{1,a}(\mathbf{k}_-)\\ \phi_{2,a}(\mathbf{k}_+)\end{pmatrix}, \tag{4}$$

written as linear combinations of $\phi_{1,a}(\mathbf{k}_-)$ and $\phi_{2,a}(\mathbf{k}_+)$. Expressions for the coefficients $u_{\pm\alpha}(\mathbf{k}_\perp)$ and $u_{\pm\beta}(\mathbf{k}_\perp)$ are found in [40]. The absolute minimum of all eigenvalues, where Bose-Einstein condensation occurs, depends on parameters q and Ω, and is found in the lower band α. We locate the minima of these energy bands by extremizing with respect to k_x. We work with dimensionless variables and set k_T as the unit of momentum and $E_T=\hbar^2k_T^2/(2m)$ as the unit of energy. The scaled parameters are $\tilde{q}=q/E_T$, $\tilde{\Omega}=\Omega/E_T$, and $\tilde{\mathbf{k}}_\perp=\mathbf{k}_\perp/k_T$.

In Fig. 2, we show the phase diagram of $\tilde{q}$ versus $\tilde{\Omega}$ arising from Eq. (3). The dashed-green line corresponds to the phase boundary $\tilde{q}_c(\tilde{\Omega})=\tilde{\Omega}^2$ for $\tilde{\Omega}<1/2$, that separates an easy-axis nematic BEC at $\tilde{\mathbf{k}}_\perp=\mathbf{0}$ for spin component $a=0$, when $\tilde{q}>\tilde{q}_c(\tilde{\Omega})$, from a double-well easy-plane nematic BEC for spin components $a=\pm1$, when $\tilde{q}<\tilde{q}_c(\tilde{\Omega})$. The dotted-red line describes the phase boundary $\tilde{q}_c(\tilde{\Omega})=\tilde{\Omega}-1/4$ for $\tilde{\Omega}>1/2$, that separates an easy-axis BEC at $\tilde{\mathbf{k}}_\perp=\mathbf{0}$ for spin component $a=0$, when $\tilde{q}>\tilde{q}_c(\tilde{\Omega})$, from a single-well easy-plane nematic BECs for spin components $a=\pm1$, when $\tilde{q}<\tilde{q}_c(\tilde{\Omega})$. The solid-blue line $\tilde{\Omega}=1/2$ separates the easy-plane nematic BECs in the α band into two sectors: (a) a double-well phase where condensation occurs at finite momenta $(\tilde{k}_x,\tilde{k}_y)=(\pm\tilde{k}_0,0)$, with $\tilde{k}_0=\sqrt{1/4-\tilde{\Omega}^2}$, and (b) a single-well phase where condensation occurs at zero momentum $\tilde{\mathbf{k}}_\perp=\mathbf{0}$. The solid-black dot at coordinates $(\tilde{q},\tilde{\Omega})=(1/4,1/2)$ represents a triple point.

Next, we discuss the interaction Hamiltonian $\hat{H}_{\rm int}=\hat{H}_0+\hat{H}_2$. The first term is the spin-independent interaction $\hat{H}_0=(c_0/2L_\perp^2)\tilde{H}_0$, with

$$\tilde{H}_0=\sum_{\substack{\mathbf{k}_\perp\mathbf{k}'_\perp\mathbf{p}_\perp\\ aa'\{n_i\}}}C_{\{n_i\}}\Lambda^{\dagger aa'}_{n_1n_2}(\mathbf{k}_{p-},\mathbf{k}'_{p+})\Lambda^{a'a}_{n_3n_4}(\mathbf{k}'_{p-},\mathbf{k}_{p+}), \tag{5}$$

where the subscripts $\{n_i\}$ denote the set of trapped states with quantum numbers (n_1,n_2,n_3,n_4) that label the coefficients $C_{\{n_i\}}=\int dz\varphi^*_{n_1}(z)\varphi^*_{n_2}(z)\varphi_{n_3}(z)\varphi_{n_4}(z)$. In Eq. (5),

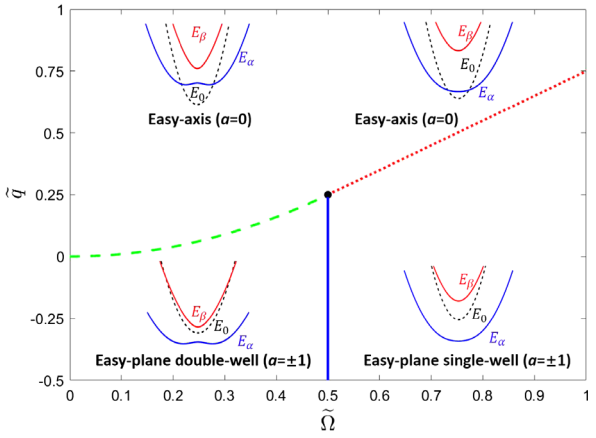

FIG. 2. Phase diagram of spin-1 Bose-Einstein condensates with nematic-orbit coupling. Shown are the ground state energies of Eq. (3) in the $\tilde{q}$ versus $\tilde{\Omega}$ plane. The diagram is separated into three regions as discussed in the text. The modified band structures are shown at four special coordinates $(\tilde{q}=0.75, \tilde{\Omega}=0.25)$, $(\tilde{q}=0.75, \tilde{\Omega}=0.75)$, $(\tilde{q}=-0.30, \tilde{\Omega}=0.25)$, and $(\tilde{q}=-0.30, \tilde{\Omega}=0.75)$.

the momenta are $\mathbf{k}_{p\pm}=\mathbf{k}_\perp \pm \mathbf{p}_\perp/2$ and $\mathbf{k}'_{p\pm}=\mathbf{k}'_\perp \pm \mathbf{p}_\perp/2$, and the operators are

$$\Lambda^{\dagger aa'}_{n_1n_2}(\mathbf{k}_{p-},\mathbf{k}'_{p+})=\phi^\dagger_{n_1,a}(\mathbf{k}_{p-})\phi^\dagger_{n_2,a'}(\mathbf{k}'_{p+}),$$
$$\Lambda^{a'a}_{n_3n_4}(\mathbf{k}'_{p-},\mathbf{k}_{p+})=\phi_{n_3,a'}(\mathbf{k}'_{p-})\phi_{n_4,a}(\mathbf{k}_{p+}). \quad (6)$$

In the interaction Hamiltonian, the second term is the spin-dependent interaction $\hat{H}_2=(c_2/2L_\perp^2)\tilde{H}_2$, with

$$\tilde{H}_2=\sum_{\substack{\mathbf{k}_\perp\mathbf{k}'_\perp\mathbf{p}_\perp\\ aa'bb'\{n_i\}}} C_{\{n_i\}}\hat{\mathbf{J}}^{ab}_{n_1n_4}(\mathbf{k}_{p-},\mathbf{k}_{p+})\cdot\hat{\mathbf{J}}^{a'b'}_{n_2n_3}(\mathbf{k}'_{p+},\mathbf{k}'_{p-}), \quad (7)$$

where the vector operators

$$\hat{\mathbf{J}}^{ab}_{n_1n_4}(\mathbf{k}_{p-},\mathbf{k}_{p+})=\phi^\dagger_{n_1,a}(\mathbf{k}_{p-})\hat{\mathbf{F}}_{ab}\phi_{n_4,b}(\mathbf{k}_{p+}),$$
$$\hat{\mathbf{J}}^{a'b'}_{n_2n_3}(\mathbf{k}'_{p+},\mathbf{k}'_{p-})=\phi^\dagger_{n_2,a'}(\mathbf{k}'_{p+})\hat{\mathbf{F}}_{a'b'}\phi_{n_3,b'}(\mathbf{k}'_{p-}), \quad (8)$$

contain the spin-1 matrices $\hat{\mathbf{F}}$.

The Hamiltonians $\hat{H}_{\rm IP}+\hat{H}_{\rm int}$ preserve the *magnetization* $m_z=n_{+1}-n_{-1}$, where $n_{\pm1}$ is the density of bosons with spin component $a=\pm1$, that is, m_z is a conserved quantity of the total Hamiltonian. From now on, we consider only $m_z=0$, in which case a phase transition occurs at $\tilde{q}_c=0$ between the easy-plane nematic state $|\zeta_P\rangle$ $(\tilde{q}<\tilde{q}_c)$ with spin densities $n_0=0$, $n_{+1}=n_{-1}\neq0$, and the easy-axis nematic state $|\zeta_A\rangle$ $(\tilde{q}>\tilde{q}_c)$ with spin densities $n_0\neq0$, $n_{+1}=n_{-1}=0$, as shown in Fig. 2, when $\tilde{\Omega}=0$ [1,14,19,21,23].

The effects of nematic-orbit coupling are also present in the collective excitations. First, we investigate the easy-axis nematic phase, where condensation occurs at $\tilde{\mathbf{k}}_\perp=\mathbf{0}$ for spin projection $a=0$. The Bogoliubov excitation spectrum is then identical to a scalar condensate, $\varepsilon_b(\mathbf{k}_\perp)=[\varepsilon_{\mathbf{k}}(\varepsilon_{\mathbf{k}}+2c_0n_c)]^{1/2}$, where n_c is the total particle density and $\varepsilon_{\mathbf{k}}=\hbar^2k_\perp^2/(2m)$ is the kinetic energy.

Next, we consider the easy-plane nematic phase in the single-well regime when $\tilde{q}\ll\tilde{\Omega}-1/4$ and $\tilde{\Omega}>0.5$. We write the field operators $\phi_{n,a}$ in terms of $\chi_{a\alpha},\chi_{a\beta}$ as shown in [40]. Condensation occurs at $\tilde{\mathbf{k}}_\perp=\mathbf{0}$ for the α band only, thus we drop the α index from our notation. The resulting Bogoliubov Hamiltonian is

$$\hat{H}=G_{\rm sw}+\frac{1}{2}\sum_{\mathbf{k}\neq0}\mathbf{X}^\dagger_{\mathbf{k}}\begin{pmatrix}\mathbf{E}_1 & \mathbf{D}\\ \mathbf{D}^\dagger & \mathbf{E}_{\bar{1}}\end{pmatrix}\mathbf{X}_{\mathbf{k}}. \quad (9)$$

The matrices for spin-preserving processes are

$$\mathbf{E}_a=\begin{pmatrix}E_g(\mathbf{k}_\perp)+c & fe^{i2\Phi_a}\\ fe^{-i2\Phi_a} & E_g(\mathbf{k}_\perp)+c\end{pmatrix}, \quad (10)$$

where $a=\{+1,-1\}$ is represented by $\{1,\bar{1}\}$, $E_g(\mathbf{k}_\perp)=E_\alpha(\mathbf{k}_\perp)-E_\alpha(0)$ is a measure of the excitation energy of independent particles with respect to the minimum of the α band, Φ_a is the spin-dependent phase of the condensate in the α band at $\mathbf{k}_\perp=\mathbf{0}$ and c, f are proportional to the spin-preserving interaction energy $(c_0+c_2)n_c$. The matrices for spin-flip processes are

$$\mathbf{D}=\begin{pmatrix}de^{i(\Phi_1-\Phi_{\bar{1}})} & ge^{i(\Phi_{\bar{1}}+\Phi_1)}\\ ge^{-i(\Phi_1+\Phi_{\bar{1}})} & de^{-i(\Phi_1-\Phi_{\bar{1}})}\end{pmatrix}, \quad (11)$$

and $\mathbf{D}^\dagger$, where d and g are proportional to the spin-flip interaction energy $(c_0-c_2)n_c$. Last, in Eq. (9), $G_{\rm sw}$ is the ground state energy and $\mathbf{X}^\dagger_{\mathbf{k}}=[\chi^\dagger_1(\mathbf{k}_\perp)\ \chi_1(-\mathbf{k}_\perp)\ \chi^\dagger_{\bar{1}}(\mathbf{k}_\perp)\ \chi_{\bar{1}}(-\mathbf{k}_\perp)]$ is a vector operator, where $\chi^\dagger_a$ represents the creation operator in the α band.

The positive eigenvalues in units of E_T are

$$\tilde{\epsilon}_{b,1}(\mathbf{k}_\perp)=\sqrt{[\tilde{E}_g(\mathbf{k}_\perp)+(\tilde{c}+\tilde{d})]^2-(\tilde{f}+\tilde{g})^2},$$
$$\tilde{\epsilon}_{b,2}(\mathbf{k}_\perp)=\sqrt{[\tilde{E}_g(\mathbf{k}_\perp)+(\tilde{c}-\tilde{d})]^2-(\tilde{f}-\tilde{g})^2}, \quad (12)$$

where $\tilde{E}_g(\mathbf{k}_\perp)=E_g(\mathbf{k}_\perp)/E_T$ is a dimensionless independent-particle energy, $\tilde{c}=(c_0+c_2)n_cA_\alpha(\mathbf{k}_\perp)/(4E_T)$, $\tilde{f}=(c_0+c_2)n_cB_\alpha(\mathbf{k}_\perp)/(4E_T)$ are dimensionless spin-preserving interaction energies and $\tilde{d}=(c_0-c_2)n_cA_\alpha(\mathbf{k}_\perp)/(4E_T)$, $\tilde{g}=(c_0-c_2)n_cB_\alpha(\mathbf{k}_\perp)/(4E_T)$, are dimensionless spin-flip interaction energies. Here, $A_\alpha(\mathbf{k}_\perp)=5/2+|\tilde{\Omega}|/[\sqrt{\tilde{k}_x^2+\tilde{\Omega}^2}]$ and $B_\alpha(\mathbf{k}_\perp)=2+3|\tilde{\Omega}|/[2\sqrt{\tilde{k}_x^2+\tilde{\Omega}^2}]$ describe the anisotropic nature of the interactions induced by the nematic-orbit coupling. When $\tilde{d}=\tilde{g}=0$, that is, $c_0=c_2$, the matrix $\mathbf{D}$ of spin-flip processes vanishes and the spin sectors $\{1,\bar{1}\}$ are

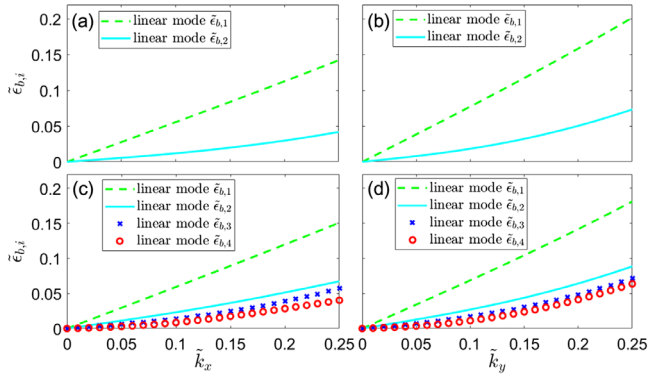

FIG. 3. Anisotropic collective excitation modes of a nematic-orbit coupled BEC. Excitation energies $\tilde{\epsilon}_{b,i}(\mathbf{k})$ for easy-plane nematic phases versus $\tilde{k}_x$ and $\tilde{k}_y$, with $\tilde{k}_z = 0$ are shown in (a) and (b) for the single-well case ($\tilde{q} = -0.3, \tilde{\Omega} = 1$) and in (c) and (d) for the double-well case ($\tilde{q} = -0.3, \tilde{\Omega} = 1/4$). The other parameters are wavelength $\lambda_T = 2\ \mu$m, particle density $n_c = 2.5 \times 10^{13}\ \mathrm{cm}^{-3}$ and interaction constants $c_0 n_c/E_T = 0.168$ and $c_2 n_c/E_T = 6.74 \times 10^{-3}$.

uncoupled leading to two degenerate linear modes at low momenta. Assuming that $c_0 > c_2 > 0$ as in ^{23}Na, we can understand a few limits from Eq. (12). In the first mode, the sum $\tilde{c} + \tilde{d}$ and $\tilde{f} + \tilde{g}$ are proportional to the spin-independent interaction parameter c_0, while in the second mode, the difference $\tilde{c} - \tilde{d}$ and $\tilde{f} - \tilde{g}$ are proportional to the spin-dependent interaction parameter c_2. Thus, the first mode is associated with density-density interactions c_0, while the second is associated with spin-spin interactions c_2. We plot the excitation spectra $\tilde{\epsilon}_{b,1}(\mathbf{k}_\perp)$ and $\tilde{\epsilon}_{b,2}(\mathbf{k}_\perp)$ versus k_x in Fig. 3(a) and versus k_y in Fig. 3(b), with c_0 and c_2 values for ^{23}Na [43].

Last, we consider the easy-plane nematic phase in the double-well region, when $\tilde{q} \ll \tilde{\Omega}^2$ and $\tilde{\Omega} < 0.5$. Condensation occurs in two degenerate minima at $\pm k_0 \hat{\mathbf{x}}$ of the α band. There are four excitation modes involving left (L) and right (R) wells and spin sectors $a = \{1, \bar{1}\}$. The Bogoliubov Hamiltonian becomes

$$\hat{H} = G_{\mathrm{dw}} + \frac{1}{2}\sum_{\mathbf{k}\neq 0} \mathbf{Y}_{\mathbf{k}}^{\dagger} \begin{pmatrix} \mathbf{M}_{LL} & \mathbf{M}_{LR} \\ \mathbf{M}_{RL} & \mathbf{M}_{RR} \end{pmatrix} \mathbf{Y}_{\mathbf{k}}, \tag{13}$$

where $\mathbf{Y}_{\mathbf{k}}^{\dagger} = [\mathbf{X}_L^{\dagger}(\mathbf{k}_\perp)\ \mathbf{X}_R^{\dagger}(\mathbf{k}_\perp)]$ is an eight-dimensional vector with four dimensional components $\mathbf{X}_j^{\dagger}(\mathbf{k}_\perp) = [\chi_{j1}^{\dagger}(\mathbf{k}_\perp)\ \chi_{j1}(-\mathbf{k}_\perp)\ \chi_{j\bar{1}}^{\dagger}(\mathbf{k}_\perp)\ \chi_{j\bar{1}}(-\mathbf{k}_\perp)]$ in the $j = \{L, R\}$ sectors, and G_{dw} is the ground state energy. The $\mathbf{M}_{ij}$ matrices are given in [40] and the excitation spectrum is obtained numerically, but a qualitative understanding is possible. In each well there are equal numbers of atoms with spin components $a = \{1, \bar{1}\}$, that is, $n_{1L} = n_{1R}$ and $n_{\bar{1}L} = n_{\bar{1}R}$. When all interactions are present and all atoms oscillate in phase, this excitation corresponds to a center-of-mass motion with linear dispersion and lowest energy at low momenta, which is also anisotropic since the effective mass is heavier along k_x. When atoms with the same spin projection a oscillate in phase in both L and R wells, but out of phase with respect to their spin projections, then a second linear mode arises with larger (larger) velocity along k_x (k_y) in comparison to the center-of-mass mode. When the spin-spin interactions are neglected and atoms with spin projection a oscillate out of phase in L and R wells they produce two degenerate linearly dispersing modes. However, when spin-spin interactions are included the degeneracy of these modes is lifted producing a linearly dispersing mode with lower (higher) energy when the relative motion of 1 and $\bar{1}$ is in (out of) phase. All four modes $\tilde{\epsilon}_{b,1}(\mathbf{k}_\perp)$, $\tilde{\epsilon}_{b,2}(\mathbf{k}_\perp)$, $\tilde{\epsilon}_{b,3}(\mathbf{k}_\perp)$, and $\tilde{\epsilon}_{b,4}(\mathbf{k}_\perp)$ of the excitation spectrum are shown in Figs. 3(c) and 3(d) for ^{23}Na parameters.

Next, we analyze manifestations of the nematic-orbit coupling in real space and focus on the easy-plane nematic phases with $n_0 = 0$ and $n_{+1} = n_{-1} \neq 0$. Far below the phase boundary $\tilde{q}_c(\tilde{\Omega})$, the effective Hamiltonian is $\hat{H}_{\mathrm{EP}} = \hat{H}'_{\mathrm{IP}} + \hat{H}_{\mathrm{I}}$, with

$$\hat{H}'_{\mathrm{IP}} = \int d^2 r_\perp \begin{pmatrix} \hat{\psi}_1^* & \hat{\psi}_2^* \end{pmatrix} \begin{pmatrix} \frac{\mathbf{p}_\perp^2}{2m} + q\hat{F}_z^2 & \Omega e^{-ik_T x}\hat{F}_z^2 \\ \Omega e^{ik_T x}\hat{F}_z^2 & \frac{\mathbf{p}_\perp^2}{2m} + q\hat{F}_z^2 \end{pmatrix} \begin{pmatrix} \hat{\psi}_1 \\ \hat{\psi}_2 \end{pmatrix}, \tag{14}$$

where $\hat{\psi}_n^* = [\psi_{n,1}^*(\mathbf{r}_\perp), \psi_{n,0}^*(\mathbf{r}_\perp), \psi_{n,\bar{1}}^*(\mathbf{r}_\perp)]$ represents the 2D condensate wave function in trap states with quantum number n. The interaction Hamiltonian is $\hat{H}_{\mathrm{I}} = \int d^3 r \hat{\mathcal{H}}_I$, where

$$\hat{\mathcal{H}}_I = \frac{c_0}{2}[|\mathbf{\Psi}_1(\mathbf{r})|^2 + |\mathbf{\Psi}_{\bar{1}}(\mathbf{r})|^2]^2 + \frac{c_2}{2}[|\mathbf{\Psi}_1(\mathbf{r})|^2 - |\mathbf{\Psi}_{\bar{1}}(\mathbf{r})|^2]^2, \tag{15}$$

with $c_0 > c_2 > 0$ as in ^{23}Na, leading to the same local condensate densities, that is, $|\mathbf{\Psi}_1(\mathbf{r})|^2 = |\mathbf{\Psi}_{\bar{1}}(\mathbf{r})|^2$.

In the single-well phase, condensation occurs in the α band at $\tilde{\mathbf{k}}_\perp = \mathbf{0}$. However, the wave function $\psi_a(\mathbf{r})$ in real space is a linear combination of momentum shifted $[\pm(k_T/2)\hat{\mathbf{x}}]$ condensates with relative phase ϑ [40], resulting in a spatial variation of the form

$$\mathbf{\Psi}_a(\mathbf{r}) = \mathcal{A}_{\mathrm{sw}} e^{-i(\vartheta/2)}[e^{i[(k_T/2)x - (\vartheta/2)]}\varphi_2(z) - e^{-i[(k_T/2)x + (\vartheta/2)]}\varphi_1(z)], \tag{16}$$

where $\varphi_{1,2}(z)$ are the trap states along the z direction and its period $\lambda_h = 2\pi/(k_T/2) = 2\lambda_T$ commensurate to the period λ_T of the periodic potential $q(\mathbf{r}, t)$. The phase $\vartheta = 0$ [40] is determined by minimization of the free energy and $\mathcal{A}_{\mathrm{sw}}$ is obtained by normalizing the condensate density

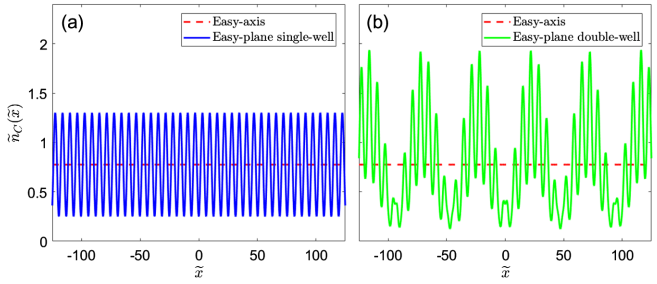

FIG. 4. Shown are easy-plane density modulations in real space for (a) single-well, with $\sigma = 0.7$, $\tilde{z} = \pi/8$ and $\tilde{\Omega} = 1$ (solid-blue line) and (b) double-well, with $\sigma = 0.7$, $\tilde{z} = \pi/8$ and $\tilde{\Omega} = 1/4$ (solid-green line). The dashed-red line shows the uniform density profile of the easy-axis nematic phase. The periodic modulation in (a) is commensurate with λ_T, while in (b) there are two periods, which are incommensurate with λ_T. In (a) the period is $\lambda_T = 2$ μm, while in (b) the short period is $\lambda_+ = 2.14$ μm, while the long period is $\lambda_- = 29.86$ μm.

$n_C(\mathbf{r}) = \sum_{a=\{1,\bar{1}\}} |\psi_a(\mathbf{r})|^2$ to the total number of condensed particles N_C [40]. Therefore, the dimensionless local condensate density $\tilde{n}_C(\tilde{x})$ at some fixed $\tilde{z}_0$, describing a easy-plane single-period nematic density wave, can be obtained by squaring the norm of Eq. (16) [40]. $\tilde{n}_C(\tilde{x})$ for $\sigma = 0.7$, $\tilde{\Omega} = 1$, and $\tilde{z} = \pi/8$ is plotted in Fig. 4(a), where $\tilde{x} = k_T x$, $\tilde{z} = (2\pi/L_z)z$ and $\sigma = N_C/N$ is the condensate fraction. It is uniform apart from the periodic variation at the lattice period λ_T.

In the double-well phase, condensation occurs in the α band at $\tilde{\mathbf{k}}_\perp = \pm\tilde{k}_0\hat{\mathbf{x}}$. Thus, the wave function $\psi_a(\mathbf{r})$ in real space is a linear combination of two single-well condensates with momenta $(k_0 \pm k_T/2)\hat{\mathbf{x}}$ and phases ϑ, ϑ_{LR} [40], resulting in a spatial variation of the form

$$\mathbf{\Psi}_a(\mathbf{r}) = \mathcal{A}'_{\mathrm{dw}} \sum_{\substack{j=\pm \\ l=\pm}} [u_{j\alpha}(l\tilde{k}_0) e^{i\{[lk_0 + j(k_T/2)]x - j(\vartheta/2) + l(\vartheta_{LR}/2)\}}] \varphi_j(z) \tag{17}$$

with two periods $\lambda_\pm = 2\pi/|k_0 \pm k_T/2|$, which are generically incommensurate with λ_T. Here, we denote $\mathcal{A}'_{\mathrm{dw}} = \mathcal{A}_{\mathrm{dw}} e^{-i(\vartheta+\vartheta_{LR}/2)}$, $\varphi_-(z) = \varphi_1(z)$ and $\varphi_+(z) = \varphi_2(z)$ for simplicity. The relative phase ϑ, ϑ_{LR} were determined by minimizing the free energy numerically [40], resulting in $\vartheta = 0$. The energy functional contains a rapid oscillation at the underlying period λ_T as the system size $L_\perp$ is varied [40]. We chose $k_T L_\perp = 250$ and $\vartheta_{LR} = 0$ to minimize the energy over this oscillation, with the results shown in Fig. 4(b). $\vartheta_{LR} = \pi$ achieved similar results for other $k_T L_\perp$. By squaring the wave function of Eq. (17), this leads to the dimensionless condensate density describing a double-period nematic density wave along x direction shown in Fig. 4(b) for $\tilde{z} = \pi/8$ (see [40]).

In conclusion, we have proposed a mechanism for the creation of nematic-orbit coupling in spin-1 condensates and uncovered their phase diagram and excitation spectra. Our work connects orbital motion of atoms to the rich physics of spin nematics, and opens up a new direction to explore strongly correlated spin-nematic states. Future work may include higher spin systems and coupling to other tensor components $\hat{\mathbf{Q}}_{ij}$. Extension to higher dimensions could allow nontrivial topology to be explored, analogous to half-quantum vortices in ordinary nematics [44], which have parallels in solid state systems [45,46].

This work was supported by NSF Grant No. 1707654. C. A. R. SdM. acknowledges the support of the International Institute of Physics, through its Visitor's Program.

*dlao7@gatech.edu

[1] D. M. Stamper-Kurn and M. Ueda, Spinor Bose gases: Symmetries, magnetism, and quantum dynamics, Rev. Mod. Phys. **85**, 1191 (2013).
[2] I. B. Spielman, Raman processes and effective gauge potentials, Phys. Rev. A **79**, 063613 (2009).
[3] G. Juzeliūnas, J. Ruseckas, and J. Dalibard, Generalized Rashba-Dresselhaus spin-orbit coupling for cold atoms, Phys. Rev. A **81**, 053403 (2010).
[4] Y. J. Lin, K. Jiménez-García, and I. B. Spielman, Spin-orbit-coupled Bose-Einstein condensates, Nature (London) **471**, 83 (2011).
[5] M. Chapman and C. Sá de Melo, Atoms playing dress-up, Nature (London) **471**, 41 (2011).
[6] S.-C. Ji, J.-Y. Zhang, L. Zhang, Z.-D. Du, W. Zheng, Y.-J. Deng, H. Zhai, S. Chen, and J.-W. Pan, Experimental determination of the finite-temperature phase diagram of a spin-orbit-coupled Bose gas, Nat. Phys. **10**, 314 (2014).
[7] J.-R. Li, J. Lee, W. Huang, S. Burchesky, B. Shteytnas, F. C. Top, A. O. Jamison, and W. Ketterle, A stripe phase with supersolid properties in spin-orbit-coupled Bose-Einstein condensates, Nature (London) **543**, 91 (2017).
[8] H. Zhai, Degenerate quantum gases with spin-orbit coupling: A review, Rep. Prog. Phys. **78**, 026001 (2015).
[9] M. DeMarco and H. Pu, Angular spin-orbit coupling in cold atoms, Phys. Rev. A **91**, 033630 (2015).
[10] D. Zhang, T. Gao, P. Zou, L. Kong, R. Li, X. Shen, X. Chen, S. Peng, M. Zhan, H. Pu, and K. Jiang, Ground-State Phase Diagram of a Spin-orbital-angular-momentum Coupled Bose-Einstein Condensate, Phys. Rev. Lett. **122**, 110402 (2019).
[11] S. Kolkowitz, S. L. Bromley, T. Bothwell, M. L. Wall, G. E. Marti, A. P. Koller, X. Zhang, A. M. Rey, and J. Ye, Spin-orbit-coupled Fermions in an Optical Lattice Clock, Nature (London) **542**, 66 (2017).
[12] S. L. Bromley, S. Kolkowitz, T. Bothwell, D. Kedar, A. Safavi-Naini, M. L. Wall, C. Salomon, A. M. Rey, and J. Ye, Dynamics of interacting fermions under spin-orbit coupling in an optical lattice clock, Nat. Phys. **14**, 399 (2018).
[13] D. L. Campbell, R. M. Price, A. Putra, A. Valdés-Curiel, D. Trypogeorgos, and I. B. Spielman, Magnetic phases of spin-1 spin-orbit-coupled Bose gases, Nat. Commun. **7**, 10897 (2016).

[14] J. Stenger, S. Inouye, D. M. Stamper-Kurn, H.-J. Miesner, A. P. Chikkatur, and W. Ketterle, Spin domains in ground-state Bose-Einstein condensates, Nature (London) **396**, 345 (1998).
[15] T. Ohmi and K. Machida, Bose-Einstein condensation with internal degrees of freedom in alkali atom gases, J. Phys. Soc. Jpn. **67**, 1822 (1998).
[16] M. Snoek and F. Zhou, Microscopic wave functions of spin-singlet and nematic Mott states of spin-one bosons in high-dimensional bipartite lattices, Phys. Rev. B **69**, 094410 (2004).
[17] A. Imambekov, M. D. Lukin, and E. Demler, Spin-exchange interactions of spin-one bosons in optical lattices: Singlet, nematic, and dimerized phases, Phys. Rev. A **68**, 063602 (2003).
[18] F. Zhou, M. Snoek, J. Wiemer, and I. Affleck, Magnetically stabilized nematic order: Three-dimensional bipartite optical lattices, Phys. Rev. B **70**, 184434 (2004).
[19] A. T. Black, E. Gomez, L. D. Turner, S. Jung, and P. D. Lett, Spinor Dynamics in an Antiferromagnetic Spin-1 Condensate, Phys. Rev. Lett. **99**, 070403 (2007).
[20] Y. Liu, S. Jung, S. E. Maxwell, L. D. Turner, E. Tiesinga, and P. D. Lett, Quantum Phase Transitions and Continuous Observation of Spinor Dynamics in an Antiferromagnetic Condensate, Phys. Rev. Lett. **102**, 125301 (2009).
[21] E. M. Bookjans, A. Vinit, and C. Raman, Quantum Phase Transition in an Antiferromagnetic Spinor Bose-Einstein Condensate, Phys. Rev. Lett. **107**, 195306 (2011).
[22] D. Jacob, L. Shao, V. Corre, T. Zibold, L. De Sarlo, E. Mimoun, J. Dalibard, and F. Gerbier, Phase diagram of spin-1 antiferromagnetic Bose-Einstein condensates, Phys. Rev. A **86**, 061601 (2012).
[23] T. Zibold, V. Corre, C. Frapolli, A. Invernizzi, J. Dalibard, and F. Gerbier, Spin-nematic order in antiferromagnetic spinor condensates, Phys. Rev. A **93**, 023614 (2016).
[24] M. O. Borgh, J. Lovegrove, and J. Ruostekoski, Imprinting a topological interface using zeeman shifts in a atomic spinor Bose-Einstein condensate, New J. Phys. **16**, 053046 (2014).
[25] L. M. Symes and P. B. Blakie, Nematic ordering dynamics of an antiferromagnetic spin-1 condensate, Phys. Rev. A **96**, 013602 (2017).
[26] S. Kang, S. W. Seo, H. Takeuchi, and Y. Shin, Observation of Wall-Vortex Composite Defects in a Spinor Bose-Einstein Condensate, Phys. Rev. Lett. **122**, 095301 (2019).
[27] A. F. Andreev and I. A. Grishchuk, Spin Nematics, Zh. Eksp. Teor. Fiz. **87**, 467 (1984) [Sov. Phys. JETP **60**, 267 (1984)], http://www.jetp.ac.ru/cgi-bin/dn/e_060_02_0267.pdf.
[28] A. Vinit, E. M. Bookjans, C. A. R. Sá de Melo, and C. Raman, Antiferromagnetic Spatial Ordering in a Quenched One-Dimensional Spinor Gas, Phys. Rev. Lett. **110**, 165301 (2013).
[29] A. Vinit and C. Raman, Hanbury Brown-Twiss correlations and multimode dynamics in quenched, inhomogeneous density spinor Bose-Einstein condensates, New J. Phys. **20**, 095003 (2018).
[30] L. E. Sadler, J. M. Higbie, S. R. Leslie, M. Vengalattore, and D. M. Stamper-Kurn, Spontaneous symmetry breaking in a quenched ferromagnetic spinor Bose-Einstein condensate, Nature (London) **443**, 312 (2006).
[31] B. Lücke, M. Scherer, J. Kruse, L. Pezzé, F. Deuretzbacher, P. Hyllus, O. Topic, J. Peise, W. Ertmer, J. Arlt, L. Santos, A. Smerzi, and C. Klempt, Twin Matter Waves for Interferometry Beyond the Classical Limit, Science **334**, 773 (2011).
[32] C. Gross, H. Strobel, E. Nicklas, T. Zibold, N. Bar-Gill, G. Kurizki, and M. K. Oberthaler, Atomic homodyne detection of continuous-variable entangled twin-atom states, Nature (London) **480**, 219 (2011).
[33] E. M. Bookjans, C. D. Hamley, and M. S. Chapman, Strong Quantum Spin Correlations Observed in Atomic Spin Mixing, Phys. Rev. Lett. **107**, 210406 (2011).
[34] T. D. Stanescu, B. Anderson, and Victor Galitski, Spin-orbit-coupled Bose-Einstein condensates, Phys. Rev. A **78**, 023616 (2008).
[35] T.-L. Ho and S. Zhang, Bose-Einstein Condensates with Spin-Orbit Interaction, Phys. Rev. Lett. **107**, 150403 (2011).
[36] Y. Li, L. P. Pitaevskii, and Sandro Stringari, Quantum Tricriticality and Phase Transitions in Spin-Orbit-Coupled Bose-Einstein Condensates, Phys. Rev. Lett. **108**, 225301 (2012).
[37] T. Ozawa and G. Baym, Stability of Ultracold Atomic Bose Condensates with Rashba Spin-Orbit Coupling against Quantum and Thermal Fluctuations, Phys. Rev. Lett. **109**, 025301 (2012).
[38] Y. Li, G. I. Martone, L. P. Pitaevskii, and S. Stringari, Superstripes and the Excitation Spectrum of a Spin-orbit-coupled Bose-Einstein Condensate, Phys. Rev. Lett. **110**, 235302 (2013).
[39] D. Yamamoto, I. B. Spielman, and C. A. R. Sá de Melo, Quantum phases of two-component bosons with spin-orbit coupling in optical lattices, Phys. Rev. A **96**, 061603(R) (2017).
[40] See Supplemental Material at http://link.aps.org/supplemental/10.1103/PhysRevLett.124.173203 for more details, which includes Refs. [41] and [42].
[41] P. Böhi, M. F. Riedel, J. Hoffrogge, J, Reichel, T. W. Hänsch, and P. Treutlein, Coherent manipulation of Bose-Einstein condensates with state-dependent microwave potentials on an atom chip, Nat. Phys. **5**, 592 (2009).
[42] F. Gerbier, A. Widera, S. Fölling, O. Mandel, and I. Bloch, Resonant control of spin dynamics in ultracold quantum gases by microwave dressing, Phys. Rev. A **73**, 041602(R) (2006).
[43] T.-L. Ho, Spinor Bose Condensates in Optical Traps, Phys. Rev. Lett. **81**, 742 (1998).
[44] S. W. Seo, S. Kang, W. J. Kwon, and Y. Shin, Half-Quantum Vortices in an Antiferromagnetic Spinor Bose-Einstein Condensate, Phys. Rev. Lett. **115**, 015301 (2015).
[45] K. G. Lagoudakis, T. Ostatnický, A. V. Kavokin, Y. G. Rubo, R. André, and B. Deveaud-Plédran, Observation of half-quantum vortices in an exciton-polariton condensate, Science **326**, 974 (2009).
[46] J. Jang, D. G. Ferguson, V. Vakaryuk, R. Budakian, S. B. Chung, P. M. Goldbart, and Y. Maeno, Observation of Half-Height Magnetization Steps in Sr_2RuO_4, Science **331**, 186 (2011).